



Triazole pyrimidine nucleosides as inhibitors of Ribonuclease A. Synthesis, biochemical, and structural evaluation

Vanessa Parmenopoulou^{a,†}, Demetra S.M. Chatzileontiadou^{a,†}, Stella Manta^a, Stamatina Bougiatioti^a, Panagiotis Maragozidis^a, Dimitra-Niki Gkaragkouni^a, Eleni Kaffesaki^a, Anastassia L. Kantsadi^a, Vassiliki T. Skamnaki^a, Spyridon E. Zographos^b, Panagiotis Zounpoulakis^b, Nikolaos A.A. Balatsos^{a,*}, Dimitris Komiotis^{a,*}, Demetres D. Leonidas^{a,*}

^a Department of Biochemistry and Biotechnology, University of Thessaly, 26 Ploutonos St., 41221 Larissa, Greece

^b Institute of Biology, Medicinal Chemistry & Biotechnology, National Hellenic Research Foundation, 48 Vas. Constantinou Avenue, 11635 Athens, Greece

ARTICLE INFO

Article history:

Received 24 July 2012

Revised 21 September 2012

Accepted 24 September 2012

Available online 16 October 2012

Keywords:

Ribonuclease A

Inhibition

X-ray crystallography

Triazole nucleosides

Structure-assisted inhibitor design

ABSTRACT

Five ribofuranosyl pyrimidine nucleosides and their corresponding 1,2,3-triazole derivatives have been synthesized and characterized. Their inhibitory action to Ribonuclease A has been studied by biochemical analysis and X-ray crystallography. These compounds are potent competitive inhibitors of RNase A with low μM inhibition constant (K_i) values with the ones having a triazole linker being more potent than the ones without. The most potent of these is 1-[(β -D-ribofuranosyl)-1,2,3-triazol-4-yl]uracil being with $K_i = 1.6 \mu\text{M}$. The high resolution X-ray crystal structures of the RNase A in complex with three most potent inhibitors of these inhibitors have shown that they bind at the enzyme catalytic cleft with the pyrimidine nucleobase at the B_1 subsite while the triazole moiety binds at the main subsite P_1 , where P-O5' bond cleavage occurs, and the ribose at the interface between subsites P_1 and P_0 exploiting interactions with residues from both subsites. The effect of a subsituent group at the 5-pyrimidine position at the inhibitory potency has been also examined and results show that any addition at this position leads to a less efficient inhibitor. Comparative structural analysis of these RNase A complexes with other similar RNase A–ligand complexes reveals that the triazole moiety interactions with the protein form the structural basis of their increased potency. The insertion of a triazole linker between the pyrimidine base and the ribose forms the starting point for further improvement of these inhibitors in the quest for potent ribonucleolytic inhibitors with pharmaceutical potential.

© 2012 Elsevier Ltd. All rights reserved.

1. Introduction

Ribonucleases (RNases) are endonucleases that control post-transcriptionally the RNA population in cells. RNases and in particular RNase A, have proven to be excellent model systems for the study of protein structure, folding and stability, and enzyme catalysis. In the last decade several homologues of the RNase A superfamily have been found to play an important role in human pathologies.¹ Human angiogenin (Ang), a potent inducer of neovascularization in vivo is an important target for many angiogenesis dependent diseases such as tumors and other non-neoplastic

diseases.² Eosinophil ribonucleases, eosinophil derived neurotoxin (EDN) and eosinophil cationic protein (ECP) are both involved in the immune response system and inflammatory disorders.^{3,4} The biological activity of all these RNase A homologues is linked to their enzymatic activity. Therefore, these proteins are pharmaceutical targets for the rational design of specific inhibitors to suppress their activity and hence modulate their pathological actions.

Several subsites exist within the central catalytic groove of RNases, where substrate RNA, binds. These are defined as $P_0\dots P_n$, $R_0\dots R_n$, and $B_0\dots B_n$ according to the phosphate, ribose and base of RNA that bind respectively, (n indicates the position of the group with respect to the cleaved phosphate phosphodiester bond where $n = 1$).⁵ The active site of all RNases is highly conserved in terms of sequence and structural architecture. However, specific differences in their peripheral RNA binding sites give rise to variations in their specificity towards different substrates and may provide clues for the rational design of specific ligands for each RNase. In the past, we have initiated structure assisted inhibitor design studies using as a template RNase A, and studied a variety of substrate analogues, mainly mono and diphosphate (di)nucleotides with

Abbreviations: RNase A, bovine pancreatic Ribonuclease A; PEG, poly(ethylene glycol); USP, deoxyuridine 5'-phosphate; ppA-3'-p, 5'-diphosphoadenosine 3'-phosphate.

* Corresponding authors. Tel.: +30 2410 565261; fax: +30 2410 565290 (N.A.A.B.); tel.: +30 2410 565285; fax: +30 2410 565290 (D.K.); tel.: +30 2410 565278; fax: +30 2410 565290 (D.D.L.).

E-mail addresses: balatsos@bio.uth.gr (N.A.A. Balatsos), dkom@bio.uth.gr (D. Komiotis), ddleonidas@bio.uth.gr (D.D. Leonidas).

[†] These two authors contributed equally to this work.

adenine at the 5'-position, and cytosine or uridine at the 3'-position of the scissile bond.^{6–10} All these compounds had significant number of polar groups (pyrophosphates, phosphates or sulfates) which may lead to cell impermeability and problems in their bioavailability.¹¹ Especially pyrophosphate groups could be hydrolysed by enzymes like Ap₃A and Ap₄A hydrolases^{12,13} rendering them ineffective and possibly toxic (themselves or degraded products).¹⁴ Hence, we have turned our attention towards compounds that did not have phosphate groups.

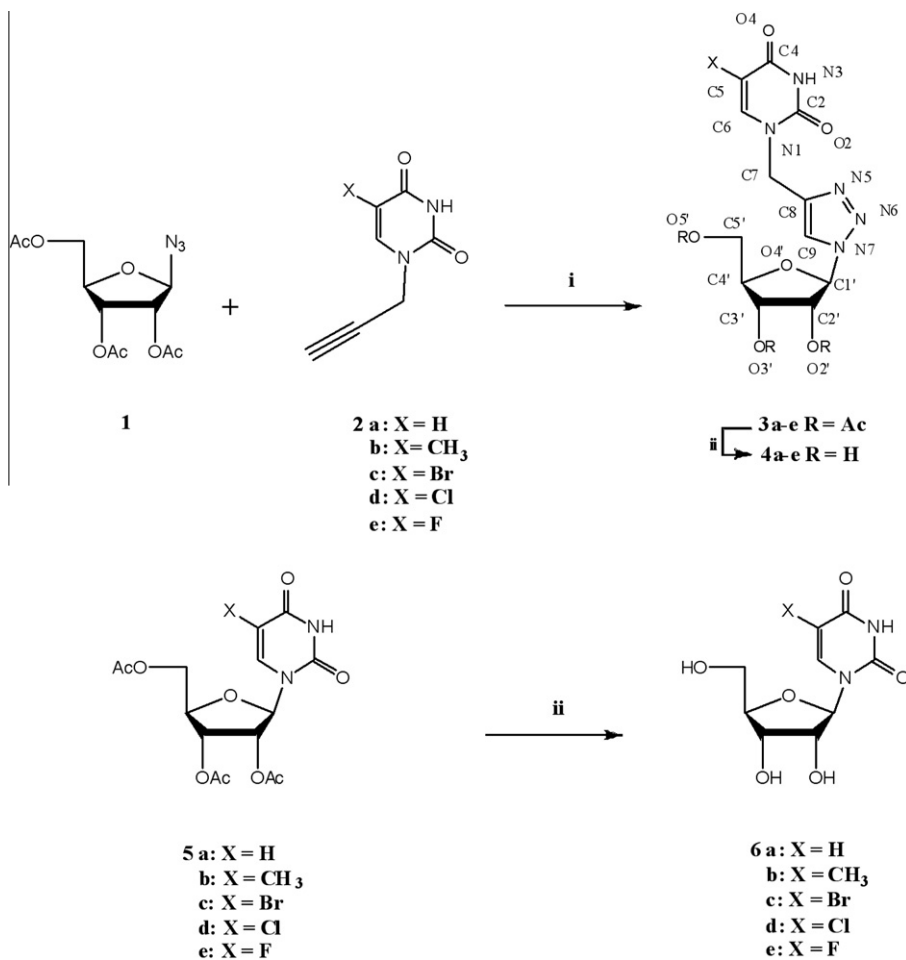
In the recent years, aminonucleosides have been identified as a new class of potent inhibitors of RNase A and angiogenin¹⁵ with K_i values in the mid μM range while the binding of the most potent of this class has been studied by X-ray crystallography.¹⁶ The binding a series of uridine and thymidine analogues that had a morpholino, piperidino, or pyrrolidino group at the 5'-position and K_i values for RNase A in the mid μM range has been also studied.¹⁷ Nucleoside-dibasic acid and nucleoside-amino acid conjugates^{18–20} have been also shown to be inhibitors of similar potency. Furthermore, two 3'-*N*-piperidine-4-carboxyl-3'-deoxy-*ara*-uridine molecules¹⁶ and three molecules of IMP⁹ bind in the catalytic site cleft of RNase A. More recently dinucleosides connected by either polar or non-polar linkers have been shown to inhibit RNase A and angiogenin with K_i values in the areas of mid- μM and upper- μM range, respectively.²¹ Despite the number of synthetic inhibitors examined thus far, the best ribonucleolytic inhibitor is pdUppA-3'p with K_i values of 27 nM, 180 nM, and 360 μM for RNase A, EDN and Ang, respectively,^{7,22,23} whereas transition state theory predicts pM values for genuine transition states.¹

Most of the more recent studies try to replace the pyrophosphate linker of the most potent inhibitors with a non-phosphoryl group.^{15,16,18,21} Thus, following the structure-guided inhibitor design approach we wanted to study the effect of the molecular length in the inhibitory potency and more specifically the effect of the distance between the nucleotide base and the ribose. This way we could correlate this distance to their potency for RNase A. Furthermore, since the 5-position of pyrimidine is amenable to additions we also wanted to explore the limitations as to the molecular size of any putative chemical group addition to this position. Herein, we have explored the binding effect of nucleoside analogs lacking any phosphate groups with the insertion of a triazole group between the ribose and the base moieties, in order to provide a variation in the inhibitor length. Our results show that the insertion of a triazole between the sugar and the base moieties increases the inhibitory potency significantly while any substitution at the 5-pyrimidine proton with halogens or a methyl group partially released the inhibitory effect of the novel nucleosides.

2. Results

2.1. Chemistry

Our first approach was focused on the synthesis of the 1,2,3-triazole 5-substituted uracil furanonucleosides **4a–e** (Scheme 1). Copper-catalyzed azide-alkyne cycloaddition (CuAAC) was utilized to couple the protected azido ribofuranose **1**²⁴ with propargyl uracil (**2a**), thymine (**2b**), 5-bromouracil (**2c**), 5-chlorouracil (**2d**) and



Scheme 1. (i) propargyl pyrimidine base, THF, H₂O, CuSO₄·5H₂O, sodium ascorbate; (ii) methanolic ammonia.

5-fluorouracil (**2e**),²⁵ in the presence of catalytic amounts of CuSO₄·5H₂O and sodium ascorbate. The Cu(I)-catalyzed [2 + 3] dipolar cycloaddition reaction occurred with full regioselectivity, resulting in the formation of the corresponding 1,4-disubstituted 1,2,3-triazoles **3a–e**. Finally, the acetyl groups of the protected nucleosides **3a–e** were cleaved using NH₃/MeOH solution to afford the corresponding free analogues **4a–e**, in very good yields (74–83%).

The current study also describes an effective and high-yield approach for the preparation of C-5 substituted uridines **6a–e** using a domestic microwave oven and adapting the typical two step Vorbruggen coupling²⁶ into a 3 min one pot reaction. Therefore, condensation of the commercially available 1,2,3,5-tetra-*O*-acetyl-β-D-ribofuranose with 5-fluorouracil, 5-chlorouracil, 5-bromouracil, uracil and thymine furnished the protected furanonucleosides **5a–e**, in the presence of trimethylsilyl trifluoromethanesulfonate, as catalyst.²⁶ The participation of 2'-acetoxy group led to the exclusive formation of the β-anomers **5**. Finally, removal of all *O*-acetyl protecting groups of **5a–e** with saturated methanolic ammonia, afforded the target unprotected nucleosides **6a–e**, in quantitative yields (85–92%).

All new compounds were well-characterized by NMR and UV spectroscopy, mass spectrometry and elemental analysis. The structure elucidation of the newly synthesized 1-(β-D-ribofuranosyl)-1,2,3-triazole nucleosides, was made on the basis of their spectroscopic data. According to ¹H NMR spectra of the 'click' products the newly formed triazole proton was observed at 7.91–7.94 ppm for analogues **3a–e** and 8.27–8.35 ppm for analogues **4a–e**.

2.2. Enzyme activity

We have evaluated the effect of the novel nucleoside analogs bearing a triazole-ring between the ribose and the sugar moieties and also lacking any phosphate groups (Fig. 1). Kinetic analysis revealed that compound **4a** could efficiently inhibit RNase A in a competitive mode with $K_i = 1.6 \mu\text{M}$. The same nucleoside without the triazole group, **6a**, inhibited the enzyme following again competitive kinetics, but the K_i value was 28.5 μM. This result shows that the distance between the sugar and the base moieties of the nucleoside is important for inhibitory potency, as the insertion of a triazole group ameliorated the inhibitory effect of the nucleoside. We further designed and synthesized nucleoside analogs with substitutions at the 5-position of the base moiety. This position is important for activity modulation and the substitution with halogens has been widely used in modern medicinal chemistry.²⁷ We therefore substituted the proton at 5-position with Br, Cl or F resulting to compounds **4c**, **4d** or **4e**, respectively. Detailed kinetic analysis of the inhibitory potencies of **4d** or **4e** against RNase A revealed that the K_i values were, 94.76 ± 8.73 and $30.85 \pm 4.44 \mu\text{M}$, respectively, while 50 μM of **4c** produced 20% inhibition of the enzymatic activity (Table 1). The analysis showed that the halogen substitution resulted to partial release of the inhibition, and the bulkier the halogen the greater the K_i value and the less efficient the inhibition. When the same experiments were performed with the nucleoside analogs lacking the triazole ring, (compounds **6a–e**), the calculated K_i values were following the same potency pattern as the triazole-bearing ones (Table 1). We also substituted the 5-proton with a methyl group, which is less polar than the halogens, in both triazole and non-triazole nucleosides (**4b** and **6b**, respectively). In this case, the K_i value for **4b** was $25.8 \pm 2.4 \mu\text{M}$, while for **6b** was $44.1 \pm 6.4 \mu\text{M}$, showing again that the triazole group is important for efficient inhibition. For either the triazole or non-triazole methyl-substituted nucleoside, the K_i values were higher than the unsubstituted nucleosides (Table 1), but lower than almost all the 5-halogen substituted ones.

Conclusively, the previous results show that the presence of the triazole group between the sugar and the base of the inhibitor is of primary importance for efficient inhibition, while adding a substituent at 5-position of the base decreases potency.

2.3. X-ray crystallography

To elucidate the structural basis of inhibition, we have determined the crystal structure of RNase A in complex with the three most potent compounds, **4a**, **4b**, and **4e**. In the monoclinic crystal form of RNase A used in the experiments there are two protein molecules in the asymmetric unit.¹⁶ All three ligands were found bound only in one of these molecules since binding to the active site of the other RNase A molecules is impeded by crystal packing contacts. This has been also observed in previous studies^{8,16,17} and provided us with two structures one free and one inhibitor complexed, from the same crystal, facilitating thus a comparative structural analysis of the binding of each ligand to RNase A. The structures of the **4a**, **4b**, and **4e** complexes are determined at 1.7, 1.8 and 1.9 Å resolution and contain 334, 246, and 324 water molecules, respectively. Upon binding to RNase A, all inhibitor molecules adopt similar conformations and bind similarly at the active site by anchoring the uracil at the B₁ subsite like previous pyrimidine inhibitors.^{5,7,8,10} The primary functional component of this subsite is Thr45, forms two hydrogen bonds with pyrimidine: its main-chain NH donates a hydrogen to O2 of the uracil while its Oγ1 donates a hydrogen to N3 of uracil (Fig. 2). The phenyl group of Phe120 and His12 Cε1 on one side, and Val43 and Asn44 on the opposite side of the pyrimidine, lie in van der Waals contact distance from the ring stabilizing its binding (Fig. 2). The triazole moiety is involved in an extensive hydrogen bond interactions network with protein residues His12, Lys41 and Gln11 (Fig. 2) at subsite P₁, (Table 2) while the ribose binds at the far end of subsite P₁ hydrogen-bonding to His119, Gln11 and Lys7 (subsite P₂). The 5-methyl group of **4b** is involved in van der Waals interactions with Asp121. The 5-fluorine of **4e** forms halogen bonds with NZ of Lys66 (subsite P₀) and the carbonyl oxygen of Asp121 (Table 2; Fig. 2).

Upon binding to RNase A, inhibitor molecules become partly buried. The solvent accessibilities of the free ligand molecules **4a**, **4b**, and **4e** are 488, 507, and 517 Å², respectively. When bound these molecular surfaces shrink to 134, 165, and 154 Å², respectively. This indicates that approximately 70% of the ligand molecules surfaces become buried. Compounds **4a**, **4b**, and **4e** on binding to RNase A, make a total of 14, 12 and 15 hydrogen bonds, respectively and 72, 55 and 61 van der Waals interactions, respectively (**4a**:11 nonpolar/nonpolar, 45 polar/nonpolar, 16 polar/polar; **4b**:8 nonpolar/nonpolar, 36 polar/nonpolar, 11 polar/polar; **4e**:10 nonpolar/nonpolar, 37 polar/nonpolar, 14 polar/polar) (see Supplementary data).

3. Discussion

The hydrogen bond and the van der Waals interactions of the triazole moiety seem to form the structural basis of the increased potency of these compounds in comparison to the ones that lack this moiety (Table 1). Structural comparison of the three triazole pyrimidine nucleoside protein complexes with the RNase A–U5P complex¹⁰ (Fig. 3) reveals that although they bind with their uracil at the B₁ subsite in a similar structural mode the rest of the molecules follow a different binding pattern, which could be attributed to the introduction of the triazole moiety in the pyrimidine nucleosides. Thus while in the RNase A–U5P complex¹⁰ the phosphoribose moiety binds away from subsite P₁ pointing to the solvent, the triazole nucleosides bind at the core of the enzyme active site (subsites B₁–R₁–P₁). There, they exploit more protein interactions than U5P and

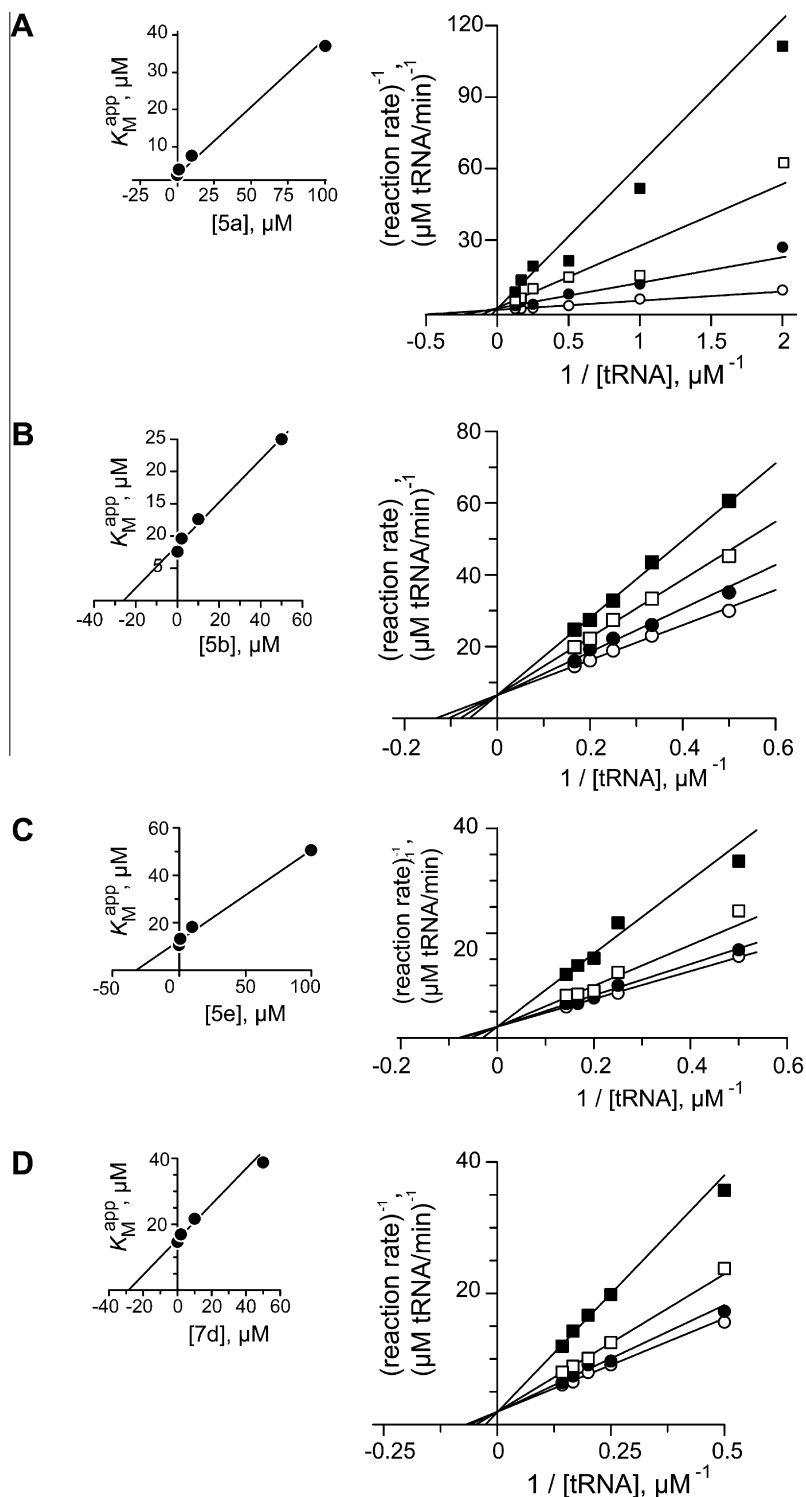


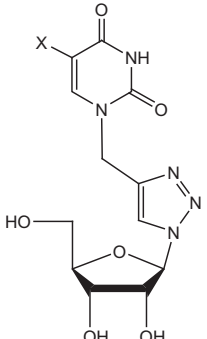
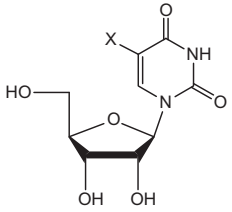
Figure 1. Pyrimidine and triazole pyrimidine nucleosides are competitive inhibitors of RNase A. Double reciprocal plots of enzyme assays are shown for nucleosides **4a** (A), **4b** (B), **4c** (C) and **6e** (D). **6e** is a pyrimidine nucleoside without a triazole ring. The nucleoside concentrations are 0 (\circ), 1 (\bullet), 10 (\square) and 50 (\blacksquare) μM , except (A) and (C) where (\blacksquare) is 100 μM . RNase A concentration is 10 nM and substrate tRNA concentrations vary from 0–6 μM . Calculated K_i values are listed in Table 1. K_M^{app} versus [I] plots for the calculation of K_i values are shown on the right of each panel. Representative plots of at least three independent experiments.

hence they are more potent inhibitors with K_i values an order of magnitude lower than that of U5P ($K_i = 4 \text{ mM}$).¹⁰ Structural comparison of the binding of **4a** to that of ppA-3'-p⁶ (the most potent mononucleoside inhibitors thus far with $K_i = 240 \text{ nM}$ ²⁸) to RNase A reveals that the ribose moiety of **4a** superposes onto the pyrophosphate group in the RNase A–ppA-3'-p complex with its hydroxyl groups onto the position of the pyrophosphate oxygen atoms

providing a possible structural explanation for **4a** potency. It is however the interactions of the adenosine of ppA-3'-p with residues of the B₂ subsite which lead to the higher potency of ppA-3'-p in comparison to **4a**. This is also supported by the fact that UDP with a K_i value of 650 μM ¹⁰ is a weaker inhibitor of RNase A.

Earlier kinetic studies^{23,29,30} had demonstrated that thymidine nucleotides bind to RNase A with K_i values comparable with those

Table 1
Kinetic parameters and structures of the inhibitors

Triazole nucleoside			Nucleoside	
				
5-Substitute (-X)	Compound	K_i (μM)	Compound	K_i (μM)
H	4a	1.6 ± 0.2	6a	28.5 ± 4.5
Me	4b	25.8 ± 2.4	6b	44.1 ± 6.4
Br	4c	20% inhibition at 50 μM	6c	69.1 ± 2.1
Cl	4d	94.8 ± 8.7	6d	44.5 ± 4.6
F	4e	30.8 ± 4.4	6e	33.6 ± 2.6

of uridine inhibitors. Our results with compounds **6a–e** are in agreement with these studies since uracil (**6a**) and thymine (**6b**) compounds have similar K_i values (Table 1). Furthermore, halogen atoms do not seem to improve significantly the inhibitory potency with the fluorine compound (**6e**) being slightly better than thymine (**6b**) which in turn is almost equipotent with the chlorine compound (**6d**) while the bromine compound (**6c**) is the less potent of all, but only 2.4 times less potent than the best inhibitor (**6a**). However, with the triazole compounds it seems that the diversity of the 5-pyrimidine substituent has an impact on RNase A inhibition since the potency of these compounds ranges from 1.6 to 94.8 μM and beyond (50 μM of compound **4c** cause only 20% inhibition). In addition the triazole compound with uracil is more potent than that with a thymine. The structural superposition of the **4a**, **4b**, and **4e** complexes (Fig. 4) reveals that the addition of a methyl group in the 5-position of pyrimidine causes a tilt of the pyrimidine ring by $\sim 10^\circ$ since it is moving away from the amide nitrogen of the Lys66 side chain which also moves to a new position with respect to its position in **4a** and **4e** complexes (Fig. 4). As a result the entire inhibitor molecule is shifted by ~ 0.7 Å and hydroxyl O5' of the ribose cannot form hydrogen bond interaction with the side chain of Lys7 (Table 2). This together with the fact that **4a** forms 72 van der Waals interactions with the protein while **4b** forms 55 can offer a structural explanation for the greater potency of **4a** with respect to **4b**. Comparison of the **4a** and **4e** complexes reveals that the fluorine atom of **4e** engages in halogen bond interactions with the side chain amide of Lys66 (Table 2); interactions which are not observed in the **4a** complex. Furthermore, **4e** participates in 61 van der Waals interactions with the protein, 11 less than **4a**. It seems that these 11 van der Waals interactions are enough to counterbalance the halogen bond interactions of **4e** and the latter is 20 times less potent than **4a**. These observations show that even small modifications of the inhibitor's chemical structure can generate profound alterations in its inhibitory potency for the target protein. Nevertheless, the main conclusion is that any substitution of the 5-pyrimidine proton leads to a decrease in inhibitory potency.

Although previous studies with dinucleosides synthesized by linking two nucleosides with either a polar or a non-polar linker²¹ led to potent inhibitors with K_i values between 59 and 544 μM for RNase A. However, the introduction of a polar linker between the

base and the ribose (as opposed between the 3'-and the 5' positions of the two ribose molecules of a dinucleotide) produced more potent ribonuclease inhibitors. This encourages following this route in our structure assisted inhibitor design approach. Comparative structural analysis of the RNase A in complex with **4a**, **4b**, and **4e** with other RNase A–ligand complexes, suggests ways to improve their potency and this study is the starting point for the design of better inhibitors. Thus, we are currently aiming to introduce an additional triazole ring at the 3'-position of the ribose of **4a**, to link a second heterocyclic base with the nucleosidic moiety, yielding to more potent inhibitors.

4. Experimental section

4.1. Chemistry. Materials and general methods

Thin layer chromatography (TLC) was performed on Merck pre-coated 60F254 plates. Reactions were monitored by TLC on silica gel, with detection by UV light (254 nm) or by charring with sulfuric acid. Flash column chromatography was performed using silica gel (240–400 mesh, Merck). UV–Vis spectra were recorded on a PG T70 UV–VIS spectrometer and mass spectra were obtained with a Micromass Platform LC (ESIMS). ^1H NMR spectra were recorded at 300 MHz on a Bruker AVANCE^{III} 300 spectrometer and ^{13}C NMR spectra at 75.5 MHz on the same spectrometer, using respectively CDCl_3 and dimethylsulfoxide- d_6 ($\text{DMSO}-d_6$) with internal tetramethylsilane (TMS). Chemical shifts (δ) were given in ppm measured downfield from TMS, and spin–spin coupling constants are in Hz. UV–Vis spectra were recorded on a PG T70 UV–VIS spectrometer and mass spectra were obtained on a Thermo Quest Finnigan AQA Mass Spectrometer (electrospray ionization). Optical rotations were measured using an Autopol I polarimeter. Acetonitrile was distilled from calcium hydride and stored over 3E molecular sieves. Microwave assisted reactions were carried out in a domestic microwave oven (Samsung-LCE 2733 GXTL) for realistic control of the microwaves operating at 850 W generating 2450 MHz frequency throughout the required time.

With the exception of CuAAC reactions, all reactions sensitive to moisture or oxygen were carried out under nitrogen environment. Azide **1**²⁴ as well as the corresponding propargyl bases **2a–e**²⁵ were prepared according to the procedures described in literature.

4.2. General procedure for preparation of the protected nucleosides **3a–e**

To a stirred mixture of azide **1**²⁴ (6.6 mmol) and the corresponding propargyl base **2a–e**²⁵ (7.6 mmol) in THF (41.6 mL), was added a solution of sodium ascorbate (3.5 mmol) and $\text{CuSO}_4 \cdot 5\text{H}_2\text{O}$ (0.84 mmol) in H_2O (41.6 mL). The reaction mixture was refluxed for 2 h and then cooled. After being treated with MeOH and concentrated, the residue was purified by flash chromatography (EtOAc) to give the desired analogues **3a–e** as white solids.

4.2.1. 1-[(2',3',5'-Tri-*O*-acetyl- β -D-ribofuranosyl)-1,2,3-triazol-4-yl]uracil (**3a**)

Yield 75%; $R_f = 0.28$ (EtOAc); $[\alpha]_D^{22} +2$ (c 0.20, CHCl_3); λ_{max} 265 nm (ϵ 9241); mp: 107–109 °C; ^1H NMR (300 MHz, CDCl_3): δ 8.97 (br s, 1H, NH), 7.94 (s, 1H, Triazole H), 7.50 (d, 1H, $J_{5,6} = 7.9$ Hz, H-6), 6.14 (d, 1H, $J'_{1,2} = 3.7$ Hz, H-1'), 5.79 (dd, 1H, $J = 3.9$ and 5.1 Hz, H-2'), 5.72 (d, 1H, H-5), 5.59 (t, 1H, H-3'), 5.02, 4.96 (q, AB-system, 2H, $J = 15.1$ Hz, CH_2), 4.48 (m, 1H, H-4'), 4.40 (dd, 1H, $J = 12.4$ and 3.1 Hz, H-5'), 4.24 (dd, 1H, $J = 12.4$ and 4.5 Hz, H-5'), 2.12, 2.11, 2.09 (3s, 9H, 3OAc). ^{13}C NMR (75.5 MHz, CDCl_3) δ 170.4, 169.4, 169.2, 163.2, 150.7, 144.2, 123.3, 102.8, 90.2, 81.0, 74.3, 70.6, 62.8, 43.1, 29.7, 20.7, 20.5, 20.4; ESIMS m/z :

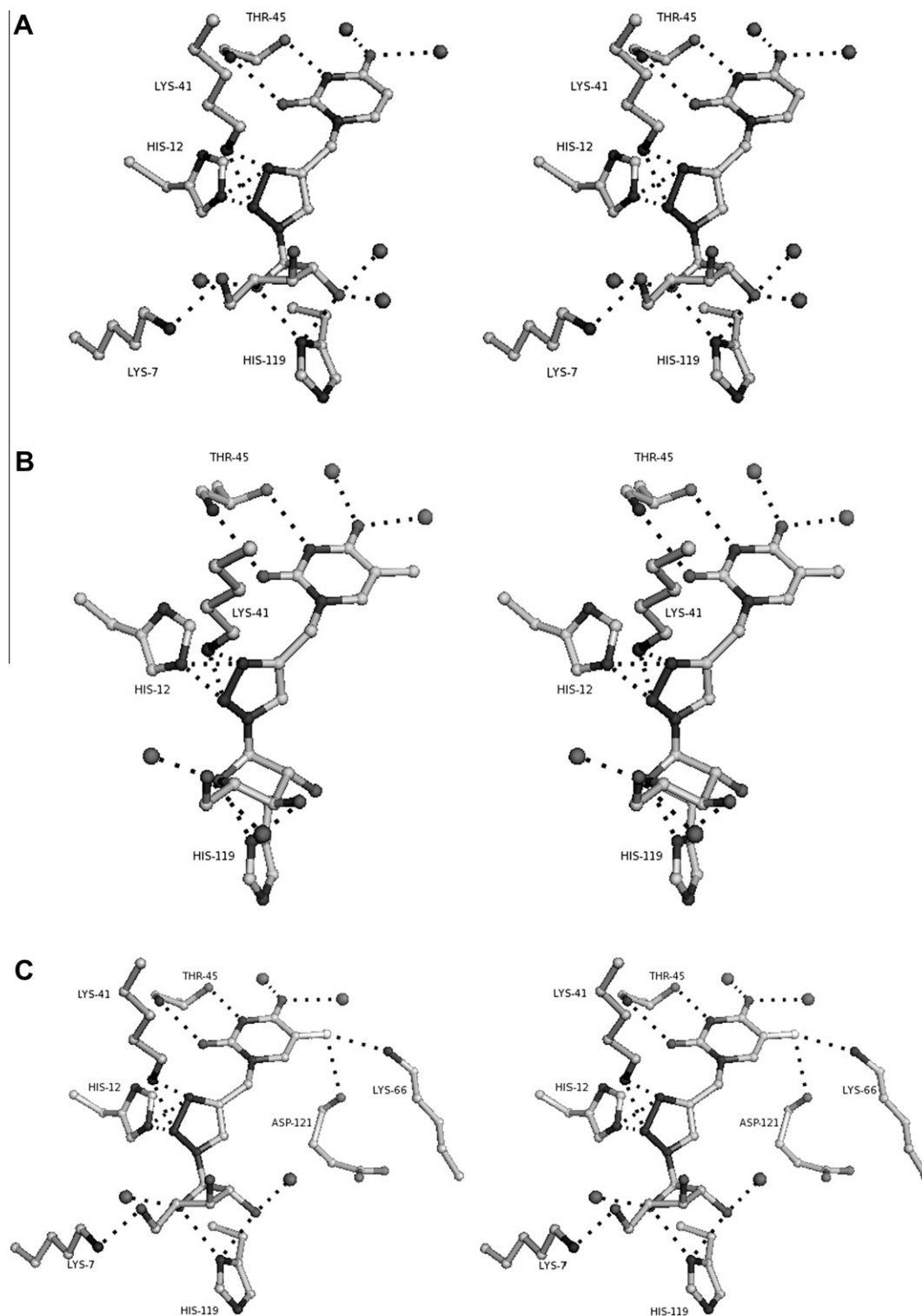


Figure 2. Stereo diagrams of the interactions between RNase A and molecule **4a** (A), **4b** (B) and **4e** (C). The side chain atoms of protein residues involved in ligand binding are shown as ball-and-stick models. Bound waters are shown as black spheres. Hydrogen bond interactions are represented as dashed lines.

452.42 [M+H]⁺. Anal. Calcd for C₁₈H₂₁N₅O₉: C, 47.90; H, 4.69; N, 15.52. Found: C, 47.73; H, 4.93; N, 15.83.

4.2.2. 1-[(2',3',5'-Tri-O-acetyl-β-D-ribofuranosyl)-1,2,3-triazol-4-yl]thymine (3b)

Yield 70%; *R*_f = 0.3 (EtOAc); [α]_D²² −4 (c 0.20, CHCl₃); λ_{max} 271 nm (ε 8030); mp: 101–102 °C; ¹H NMR (300 MHz, CDCl₃): δ 8.64 (br s,

1H, NH), 7.91 (s, 1H, Triazole H), 7.33 (s, 1H, H-6), 6.13 (d, 1H, *J*_{1,2}' = 3.7 Hz, H-1'), 5.80 (dd, 1H, *J* = 3.9 and 5.1 Hz, H-2'), 5.59 (t, 1H, H-3'), 5.00, 4.92 (q, AB-system, 2H, *J* = 15.0 Hz, CH₂), 4.48 (m, 1H, H-4'), 4.40 (dd, 1H, *J* = 12.4 and 3.0 Hz, H-5'), 4.24 (dd, 1H, *J* = 12.4 and 4.5 Hz, H-5'), 2.12, 2.11, 2.09 (3s, 9H, 3OAc), 1.91 (s, 3H, CH₃). ¹³C NMR (75.5 MHz, CDCl₃) δ 170.4, 169.4, 169.2, 163.9, 150.8, 142.4, 140.1, 123.2, 111.4, 90.3, 81.0, 74.3, 70.6,

Table 2

Potential hydrogen bond interactions of the inhibitors when bound to RNase A in the crystal

Inhibitor atom ^a	Protein atom	4a	4b	4e
O2'	His119 ND1	2.3	2.8	2.3
	Wat215	2.2	–	–
	Wat306	3.1	–	3.3
O4'	His119 ND1	3.0	2.9	3.2
	Wat22	2.5	3.0	2.8
O5'	Lys7 NZ	2.4	–	2.4
	Wat226	–	2.6	–
N3	Thr45 OG1	2.8	2.8	2.8
N5	His12 NE2	3.0	2.8	3.0
	Lys41 NZ	2.7	2.7	2.9
N6	His12 NE2	2.6	2.7	2.7
	Lys41 NZ	2.9	3.1	3.3
O2	Thr45 N	2.9	2.9	2.9
O4	Wat186	2.5	2.9	2.7
	Wat99	3.1	3.1	2.9
F5A	Asp121 O	–	–	3.3
	Lys66 NZ	–	–	3.1
Total		14	12	15

Water mediated interactions. Wat215 is hydrogen-bonded to Wat306, which in turn forms hydrogen bonds with Wat221. Wat221 is hydrogen-bonded to Asp121 OD1. Wat22 is hydrogen-bonded to Gln11 OE1, Wat16, which in turn forms hydrogen bond interactions with Ala4 O, and Val118 O. Wat186 is hydrogen-bonded Ser123 OG, Thr45 OG1, and Asp83 OD1. Wat99 forms hydrogen bonds with Ser123 N and Wat100. Wat100 is hydrogen-bonded to Ser123 O.

^a For ligand atom definitions see Table 1.

62.8, 42.9, 20.7, 20.5, 20.4, 12.3; ESIMS m/z : 466.39 [M+H]⁺. Anal. Calcd for C₁₉H₂₃N₅O₉: C, 49.03; H, 4.98; N, 15.05. Found: C, 49.40; H, 4.74; N, 15.32.

4.2.3. 1-[(2',3',5'-Tri-O-acetyl-β-D-ribofuranosyl)-1,2,3-triazol-4-yl]5-bromouracil (3c)

Yield 65%; R_f = 0.41 (EtOAc); $[\alpha]_D^{22}$ –24 (c 0.20, CHCl₃); λ_{max} 282 nm (ϵ 8703); mp: 90–93 °C; ¹H NMR (300 MHz, CDCl₃): δ 8.80 (br s, 1H, NH), 7.93 (s, 1H, Triazole H), 7.87 (s, 1H, H-6), 6.15 (d, 1H, $J_{1,2}' = 3.7$ Hz, H-1'), 5.79 (dd, 1H, $J = 3.9$ and 5.2 Hz, H-2'), 5.58 (t, 1H, H-3'), 5.04, 4.98 (q, AB-system, 2H, $J = 15.1$ Hz, CH₂), 4.48 (m, 1H, H-4'), 4.40 (dd, 1H, $J = 12.4$ and 3.1 Hz, H-5'), 4.25 (dd, 1H, $J = 12.4$ and 4.5 Hz, H-5'), 2.12, 2.11, 2.09 (3s, 9H, 3OAc). ¹³C NMR (75.5 MHz, CDCl₃) δ 170.4, 169.5, 169.3, 159.2,

150.2, 143.5, 141.6, 123.5, 97.2, 90.3, 81.0, 74.3, 70.6, 62.8, 43.3, 20.7, 20.5, 20.4; ESIMS m/z : 531.30 [M+H]⁺. Anal. Calcd for C₁₈H₂₀BrN₅O₉: C, 40.77; H, 3.80; N, 13.21. Found: C, 41.02; H, 3.53; N, 12.94.

4.2.4. 1-[(2',3',5'-Tri-O-acetyl-β-D-ribofuranosyl)-1,2,3-triazol-4-yl]5-chlorouracil (3d)

Yield 68%; R_f = 0.39 (EtOAc); $[\alpha]_D^{22}$ –8 (c 0.20, CHCl₃); λ_{max} 279 nm (ϵ 9402); mp: 80–82 °C; ¹H NMR (300 MHz, CDCl₃): δ 8.77 (br s, 1H, NH), 7.94 (s, 1H, Triazole H), 7.76 (s, 1H, H-6), 6.15 (d, 1H, $J_{1,2}' = 3.6$ Hz, H-1'), 5.79 (dd, 1H, $J' = 4.1$ and 5.0 Hz, H-2'), 5.58 (t, 1H, H-3'), 5.00 (t, 2H, $J = 15.7$ Hz, CH₂), 4.49 (m, 1H, H-4'), 4.40 (dd, 1H, $J = 12.4$ and 3.0 Hz, H-5'), 4.25 (dd, 1H, $J = 12.4$ and 4.5 Hz, H-5'), 2.12, 2.11, 2.10 (3s, 9H, 3OAc). ¹³C NMR (75.5 MHz, CDCl₃) δ 170.4, 169.5, 169.3, 159.1, 149.9, 141.6, 141.0, 123.4, 109.5, 90.3, 81.0, 74.3, 70.6, 62.8, 43.3, 20.7, 20.5, 20.4; ESIMS m/z : 486.85 [M+H]⁺. Anal. Calcd for C₁₈H₂₀ClN₅O₉: C, 44.50; H, 4.15; N, 14.42. Found: C, 44.68; H, 3.92; N, 14.12.

4.2.5. 1-[2',3',5'-Tri-O-acetyl-β-D-ribofuranosyl)-1,2,3-triazol-4-yl]5-fluorouracil (3e)

Yield 71%; R_f = 0.5 (EtOAc); $[\alpha]_D^{22}$ +2 (c 0.20, CHCl₃); λ_{max} 271 nm (ϵ 7718); mp: 49–51 °C; ¹H NMR (300 MHz, CDCl₃): δ 8.78 (br s, 1H, NH), 7.93 (s, 1H, Triazole H), 7.61 (d, 1H, $J_{6,F} = 5.3$ Hz, H-6), 6.15 (d, 1H, $J_{1,2}' = 3.5$ Hz, H-1'), 5.79 (dd, 1H, $J = 3.9$ and 4.9 Hz, H-2'), 5.58 (t, 1H, H-3'), 5.00, 4.94 (q, AB-system, 2H, $J = 15.2$ Hz, CH₂), 4.49 (m, 1H, H-4'), 4.40 (dd, 1H, $J = 12.4$ and 2.9 Hz, H-5'), 4.25 (dd, 1H, $J = 12.5$ and 4.5 Hz, H-5'), 2.13, 2.12, 2.10 (3s, 9H, 3OAc). ¹³C NMR (75.5 MHz, CDCl₃) δ 170.4, 169.5, 169.3, 157.2, 149.5, 142.2, 141.6, 139.1, 128.7, 123.4, 90.3, 80.9, 74.3, 70.6, 62.8, 20.7, 20.4, 20.3; ESIMS m/z : 470.39 [M+H]⁺. Anal. Calcd for C₁₈H₂₀FN₅O₉: C, 46.06; H, 4.29; N, 14.92. Found: C, 46.45; H, 4.48; N, 14.67.

4.3. General procedure for the preparation of unprotected nucleosides 4a–e

The protected nucleosides **3a–e** (1 mmol) were treated with ammonia/MeOH (saturated at 0 °C, 41.8 mL) overnight at room temperature. The solvent was evaporated under reduced pressure to afford pure **4a–e**, in 74–83% yields as white solids.

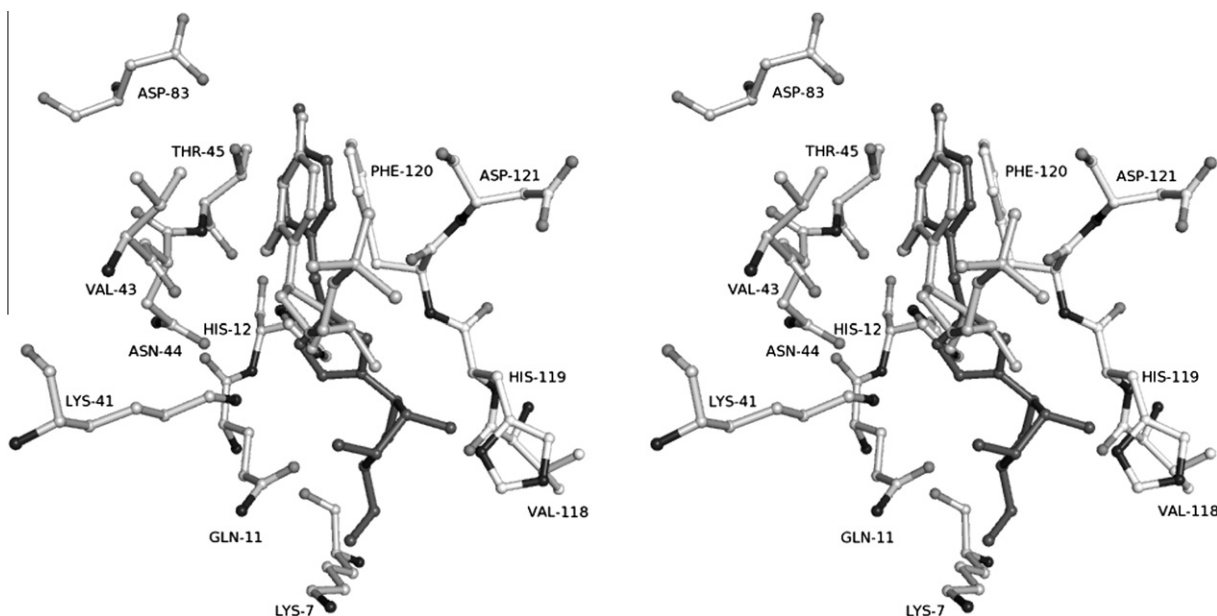


Figure 3. A stereo diagram of the RNase A–**4a** complex structure (grey) superimposed onto the RNase A–U-5'-P complex structure¹⁰ (white). Ligand molecules, **4a** and U-5'-P, are in grey and white, respectively.

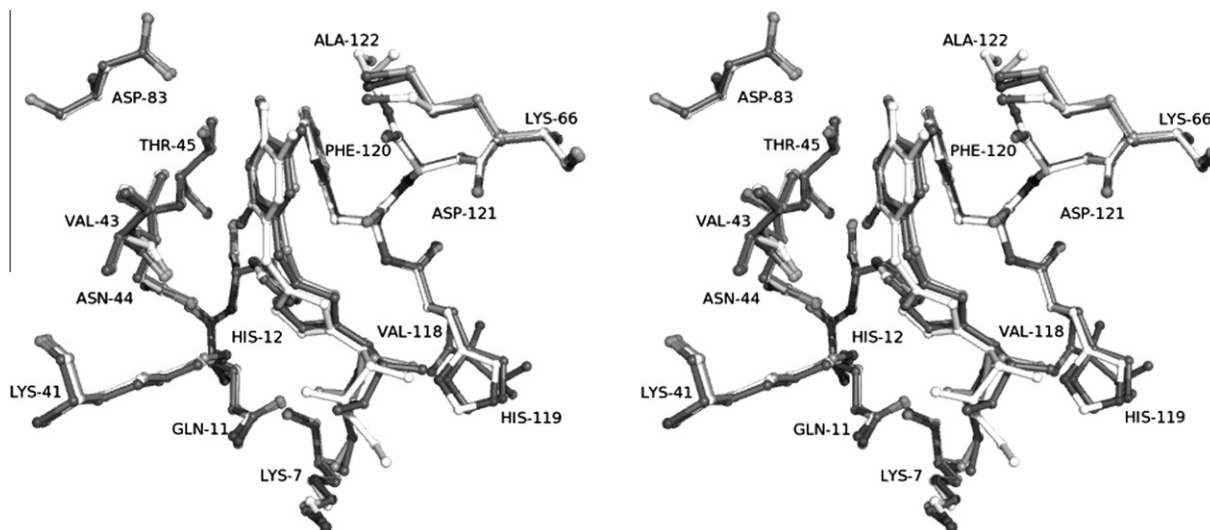


Figure 4. A stereo diagram of the with the superimposed structures of the three RNase A inhibitor complexes at the active site. Coloring scheme used for the complexes is **4a** grey, **4b** white, and **4e** black.

4.3.1. 1-[(β -D-Ribofuranosyl)-1,2,3-triazol-4-yl]uracil (**4a**)

Yield 82%; R_f = 0.25 (EtOAc/MeOH 8.5:1.5); $[\alpha]_D^{22}$ -4 (c 0.20, MeOH); λ_{max} 264 nm (ϵ 10255); mp: 97–99 °C; ^1H NMR (300 MHz, DMSO- d_6): δ 10.97 (br s, 1H, NH), 8.30 (s, 1H, Triazole H), 7.75 (d, 1H, $J_{5,6}$ = 7.9 Hz, H-6), 5.91 (d, 1H, $J_{1',2'}$ = 4.8 Hz, H-1'), 5.58 (m, 2H, H-5 and 3'-OH), 5.22 (d, 1H, $J_{2',\text{OH}2'}$ = 5.1 Hz, 2'-OH), 4.95 (m, 3H, CH₂ and 5'-OH), 4.36 (dd, 1H, J = 4.8 and 10.2 Hz, H-3'), 4.11 (dd, 1H, J = 4.6 and 9.2 Hz, H-2'), 3.96 (dd, 1H, J = 4.2 and 8.4 Hz, H-4'), 3.63–3.42 (m, 2H, H-5'). ^{13}C NMR (75.5 MHz, DMSO- d_6) δ 171.4, 163.6, 150.6, 145.4, 142.6, 122.0, 101.2, 91.9, 85.8, 74.9, 70.3, 61.2; ESIMS m/z : 326.27 [M+H]⁺. Anal. Calcd for C₁₂H₁₅N₅O₆: C, 44.31; H, 4.65; N, 21.53. Found: C, 44.19; H, 4.86; N, 21.13.

4.3.2. 1-[(β -D-Ribofuranosyl)-1,2,3-triazol-4-yl]thymine (**4b**)

Yield 78%; R_f = 0.29 (EtOAc/MeOH 8.5:1.5); $[\alpha]_D^{22}$ -8 (c 0.20, MeOH); λ_{max} 270 nm (ϵ 5184); mp: 76–78 °C; ^1H NMR (300 MHz, DMSO- d_6): δ 11.08 (br s, 1H, NH), 8.28 (s, 1H, Triazole H), 7.63 (s, 1H, H-6), 5.91 (d, 1H, $J_{1',2'}$ = 4.7 Hz, H-1'), 5.56 (d, 1H, $J_{3',\text{OH}3'}$ = 5.8 Hz, 3'-OH), 5.22 (d, 1H, $J_{2',\text{OH}2'}$ = 4.9 Hz, 2'-OH), 4.96 (t, 1H, J = 5.0 Hz, 5'-OH), 4.91 (s, 2H, CH₂), 4.36 (dd, 1H, J = 4.3 and 9.0 Hz, H-3'), 4.09 (d, 1H, H-2'), 3.96 (dd, 1H, J = 3.4 and 7.4 Hz, H-4'), 3.63–3.45 (m, 2H, H-5'), 1.76 (s, 3H, CH₃). ^{13}C NMR (75.5 MHz, DMSO- d_6) δ 164.2, 150.6, 142.7, 141.1, 122.0, 108.8, 91.9, 85.8, 74.9, 70.3, 61.2, 22.4, 11.9; ESIMS m/z : 340.33 [M+H]⁺. Anal. Calcd for C₁₃H₁₇N₅O₆: C, 46.02; H, 5.05; N, 20.64. Found: C, 46.35; H, 4.88; N, 20.52.

4.3.3. 1-[(β -D-Ribofuranosyl)-1,2,3-triazol-4-yl]5-bromouracil (**4c**)

Yield 74%; R_f = 0.4 (EtOAc/MeOH 8.5:1.5); $[\alpha]_D^{22}$ -4 (c 0.20, MeOH); λ_{max} 280 nm (ϵ 9785); mp: 176–178 °C; ^1H NMR (300 MHz, DMSO- d_6): δ 11.65 (br s, 1H, NH), 8.35 (s, 1H, Triazole H), 8.31 (s, 1H, H-6), 5.91 (d, 1H, $J_{1',2'}$ = 4.7 Hz, H-1'), 5.56 (d, 1H, $J_{3',\text{OH}3'}$ = 6.1 Hz, 3'-OH), 5.22 (d, 1H, $J_{2',\text{OH}2'}$ = 5.2 Hz, 2'-OH), 4.97 (m, 2H, CH₂ and 5'-OH), 4.37 (dd, 1H, J = 5.2 and 10.6 Hz, H-3'), 4.11 (dd, 1H, J = 4.9 and 9.5 Hz, H-2'), 3.96 (dd, 1H, J = 4.3 and 8.4 Hz, H-4'), 3.62–3.45 (m, 2H, H-5'). ^{13}C NMR (75.5 MHz, DMSO- d_6) δ 159.6, 150.0, 145.1, 142.3, 122.1, 94.9, 91.9, 85.8, 74.9, 70.3, 61.2, 42.7; ESIMS m/z : 405.19 [M+H]⁺. Anal. Calcd for C₁₂H₁₄BrN₅O₆: C, 35.66; H, 3.49; N, 17.33. Found: C, 35.91; H, 3.25; N, 17.53.

4.3.4. 1-[(β -D-Ribofuranosyl)-1,2,3-triazol-4-yl]5-chlorouracil (**4d**)

Yield 79%; R_f = 0.38 (EtOAc/MeOH 8.5:1.5); $[\alpha]_D^{22}$ -4 (c 0.20, MeOH); λ_{max} 277 nm (ϵ 7550); mp: 103–105 °C; ^1H NMR (300 MHz, DMSO- d_6): δ 10.94 (br s, 1H, NH), 8.32 (s, 1H, Triazole H), 8.28 (s, 1H, H-6), 5.91 (d, 1H, $J_{1',2'}$ = 4.8 Hz, H-1'), 5.57, 5.23 (2 br s, 2H, 3'-OH and 2'-OH), 4.96 (m, 3H, CH₂ and 5'-OH), 4.36 (t, 1H, H-3'), 4.10 (t, 1H, H-2'), 3.96 (dd, 1H, J = 4.2 and 8.4 Hz, H-4'), 3.62–3.44 (m, 2H, H-5'). ^{13}C NMR (75.5 MHz, DMSO- d_6) δ 159.4, 149.8, 142.8, 142.6, 142.3, 122.2, 106.4, 91.9, 85.7, 74.8, 70.3, 42.8; ESIMS m/z : 360.71 [M+H]⁺. Anal. Calcd for C₁₂H₁₄ClN₅O₆: C, 40.07; H, 3.92; N, 19.47. Found: C, 39.97; H, 4.19; N, 19.16.

4.3.5. 1-[(β -D-Ribofuranosyl)-1,2,3-triazol-4-yl]5-fluorouracil (**4e**)

Yield 83%; R_f = 0.32 (EtOAc/MeOH 8.5:1.5); $[\alpha]_D^{22}$ -4 (c 0.20, MeOH); λ_{max} 271 nm (ϵ 3645); mp: 63–65 °C; ^1H NMR (300 MHz, DMSO- d_6): δ 10.73 (br s, 1H, NH), 8.31 (s, 1H, Triazole H), 8.19 (d, 1H, $J_{6,F}$ = 6.6 Hz, H-6), 5.91 (d, 1H, $J_{1',2'}$ = 4.3 Hz, H-1'), 5.58, 5.24 (2 br s, 2H, 3'-OH and 2'-OH), 4.96, 4.91 (2s, 3H, 5'-OH and CH₂), 4.35 (m, 1H, H-3'), 4.10 (m, 1H, H-2'), 3.95 (m, 1H, H-4'), 3.62–3.46 (m, 2H, H-5'). ^{13}C NMR (75.5 MHz, DMSO- d_6) δ 160.5, 152.5, 145.6, 143.5, 142.0, 125.4, 95.0, 89.0, 78.2, 73.5, 64.4, 45.8; ESIMS m/z : 344.29 [M+H]⁺. Anal. Calcd for C₁₂H₁₄FN₅O₆: C, 41.99; H, 4.11; N, 20.40. Found: C, 42.35; H, 3.92; N, 20.69.

4.4. Preparation of uridines **6a–e**

A mixture of commercially available β -D-ribose tetraacetate (6.28 mmol) with pyrimidine base (8.8 mmol), 30.8 mL of acetonitrile, hexamethyldisilazane (10.9 mmol, 1.24 equiv), saccharine (0.4 mmol, 0.046 equiv) and trimethylsilyl trifluoromethanesulfonate (8.8 mmol, 1.4 equiv) was taken in a Erlenmeyer flask. The Erlenmeyer flask was placed in a microwave oven and irradiated under at low power (100 W) for 3 min. The reaction mixture was cooled at room temperature, neutralized with aqueous sodium bicarbonate, and extracted with CH₂Cl₂. The organic extract was dried over anhydrous sodium sulfate, filtered and evaporated to dryness. The residue was purified by column chromatography eluting with AcOEt/hexane 7:3, resulting in the desired nucleosides **5a–e**, in 75–82% yields. Finally, the protected nucleosides **5a–e** (1 mmol) were treated with ammonia/MeOH (saturated at 0 °C,

Table 3
Crystallographic statistics

RNase complex	4a	4b	4c
Experiment	10 mM (3 h)	10 mM (19 h)	10 mM (19 h)
Resolution (Å)	30–1.7	30–1.80	30–1.90
Outermost shell (Å)	1.79–1.70	1.9–1.8	2.0–1.9
Reflections measured	95436	157333	72335
Unique reflections	25105	22087	18814
R_{symm}^a	0.051 (0.195)	0.100 (0.441)	0.072 (0.312)
Completeness (%) ^a	96.6 (78.1)	99.7 (99.7)	99.6 (98.9)
$\langle I/\sigma \rangle^a$	15.1 (3.2)	12.4 (2.8)	12.7 (2.8)
R_{cryst}^a	0.187 (0.229)	0.199 (0.241)	0.175 (0.206)
R_{free}^a	0.237 (0.295)	0.257 (0.332)	0.236 (0.271)
No of solvent molecules	334	246	324
r.m.s. deviation from ideality			
in bond lengths (Å)	0.007	0.006	0.007
in angles (°)	1.3	1.2	1.2
Average B factor			
Protein atoms (Å ²)	16.5/18.0	16.7/16.9	17.7/18.1
(molecule A/molecule B)			
Solvent molecules (Å ²)	24.3	22.9	25.5
Ligand atoms (Å ²)	30.1	30.2	42.0
PDB entry	4G8V	4G8Y	4G90

^a Values in parentheses are for the outermost shell.

41.8 mL) overnight at room temperature. The solvent was evaporated under reduced pressure to give compounds **6a–e**, in 85–92% yields. Chemical and physical properties of the ribofuranosyl nucleosides were in agreement with previous data.^{31–35}

4.5. Enzyme kinetics

Bovine pancreatic RNase A (type XII-A), yeast tRNA and other chemicals were obtained from Sigma–Aldrich (Athens, Greece). Concentrations of the RNase A solutions were determined spectrophotometrically using absorption coefficient $\epsilon_{278.5} = 9800 \text{ M}^{-1} \text{ cm}^{-1}$ ³⁶ The Ribonuclease A activity assay used was adapted from the procedure described by Anfinsen et al.³⁷ and Slifman et al.³⁸ Briefly, yeast tRNA was solubilized in a 50 mM sodium phosphate buffer, pH 7.4 at concentrations varying from 2 μM to 7 μM . The final volume of the reaction was 300 μl . tRNA solutions were incubated at 30 °C for 10 min. 10 nM RNase A diluted in 0.1 M sodium acetate/acetic acid buffer, pH 6.0, and added to the reaction mixture. The reaction was stopped one minute later by the addition of 300 μl of fresh ice-cold solution of 40 mM lanthanum nitrate, 6% v/v perchloric acid. Stopped reactions were maintained on ice for 15 min, and insoluble tRNA was removed by centrifugation at 4 °C for 15 min at 14,500 rpm on a bench centrifuge. 50 μl of the supernatant was taken and diluted to 1 ml. The amount of cleaved tRNA was determined from the ultraviolet absorbance at 260 nm (A_{260}) of the supernatant fraction. The same procedure was repeated, by adding different concentrations of the inhibitors in the tRNA solutions as described in the text. Preliminary experiments where RNase A solutions were incubated with the inhibitors before starting the reaction did not show any difference in the reaction rate. Calculations included the following approximations: the average molecular weight (Mr) of tRNA as Mr 28,100 (75–90 ribonucleotides/tRNA molecule X Mr 341/ribonucleotide), with A_{260} of 1.0 corresponding to 40 μg of RNA.³

4.6. Crystallization, data collection and structure refinement

The protein–ligand complexes were formed by soaking native crystals of RNase A grown in the monoclinic lattice C2 as described previously⁶ with each of the compounds in a buffered solution (20 mM sodium citrate pH 5.5, 25% PEG 4000), prior to data collection (experiment conditions are shown in Table 3). X-ray diffraction data were collected on an Oxford Diffraction SuperNova

source diffractometer with a 135 mm Atlas CCD area detector using Nova microfocus Cu-K α radiation source ($\lambda = 1.54178 \text{ \AA}$) at 100 K using a cryoprotectant solution of the crystallization medium supplemented with 20% v/v 2-Methyl-2,4-pentanediol. Data processing was performed with CrysAlis^{Pro}³⁹ and scaled using SCA-LA from CCP4 program suite.⁴⁰ The crystal structure of the free RNase A¹⁶ was used as a starting model, building was performed with COOT⁴¹, and refinement using the maximum likelihood target function as implemented in the program PHENIX.⁴² Inhibitor molecules were modeled using the Dundee PRODRG server (<http://davapc1.bioch.dundee.ac.uk/programs/prodrgr/>) and they were fitted in the electron density maps by adjustment of their torsion angles during the final stages of the refinement. Details of data processing and refinement statistics are provided in Table 3. The stereochemistry of the protein residues was validated by MolProbity.⁴³ Hydrogen bonds and van der Waals interactions were calculated with the program CONTACT as implemented in CCP4⁴⁰ applying a distance cut off 3.3 and 4.0 Å, respectively. Solvent accessible areas were calculated with the program NACCESS.⁴⁴ Figures were prepared with the program Pymol.⁴⁵

Acknowledgments

We would like to thank S. Karoulias, for preliminary work with the inhibitors. This work was supported by the Hellenic General Secretariat for Research and Technology (GSRT), through a Joint Research and Technology project between Greece and France (2010–2012) and in part by the Postgraduate Programmes ‘Biotechnology–Quality assessment in Nutrition and the Environment’, ‘Application of Molecular Biology–Molecular Genetics–Molecular Markers’, Department of Biochemistry and Biotechnology, University of Thessaly.

Supplementary data

Supplementary data associated with this article can be found, in the online version, at <http://dx.doi.org/10.1016/j.bmc.2012.09.067>.

References and notes

- Loverix, S.; Steyaert, J. *Curr. Med. Chem.* **2003**, *10*, 779.
- Folkman, J. *Nat. Rev. Drug Discov.* **2007**, *6*, 273.
- Boix, E.; Torrent, M.; Sanchez, D.; Nogues, M. V. *Curr. Pharm. Biotechnol.* **2008**, *9*, 141.
- Rosenberg, H. F. *Curr. Pharm. Biotechnol.* **2008**, *9*, 135.
- Raines, R. T. *Chem. Rev.* **1998**, *98*, 1045.
- Leonidas, D. D.; Shapiro, R.; Irons, L. I.; Russo, N.; Acharya, K. R. *Biochemistry* **1997**, *36*, 5578.
- Leonidas, D. D.; Shapiro, R.; Irons, L. I.; Russo, N.; Acharya, K. R. *Biochemistry* **1999**, *38*, 10287.
- Leonidas, D. D.; Chavali, G. B.; Oikonomakos, N. G.; Chrysina, E. D.; Kosmopoulou, M. N.; Vlasi, M.; Frankling, C.; Acharya, K. R. *Protein Sci.* **2003**, *12*, 2559.
- Hatzopoulos, G. N.; Leonidas, D. D.; Kardakaris, R.; Kobe, J.; Oikonomakos, N. G. *FEBS J.* **2005**, *272*, 3988.
- Tsirkone, V. G.; Dossi, K.; Drakou, C.; Zographos, S. E.; Kontou, M.; Leonidas, D. D. *Acta Crystallogr., Sect. F: Struct. Biol. Cryst. Commun.* **2009**, *65*, 671.
- Yakovlev, G. I.; Mitkevich, V. A.; Makarov, A. A. *Mol. Biol.* **2006**, *40*, 867.
- Pace, H. C.; Garrison, P. N.; Robinson, A. K.; Barnes, L. D.; Draganescu, A.; Rosler, A.; Blackburn, G. M.; Siprashvili, Z.; Croce, C. M.; Huebner, K.; Brenner, C. *Proc. Natl. Acad. Sci. U.S.A.* **1998**, *95*, 5484.
- Swarbrick, J. D.; Buyya, S.; Gunawardana, D.; Gayler, K. R.; McLennan, A. G.; Gooley, P. R. *J. Biol. Chem.* **2005**, *280*, 8471.
- McLennan, A. G. *Pharmacol. Ther.* **2000**, *87*, 73.
- Maiti, T. K.; Soumya, D.; Dasgupta, S.; Pathak, T. *Bioorg. Med. Chem.* **2006**, *14*, 1221.
- Leonidas, D. D.; Maiti, T. K.; Samanta, A.; Dasgupta, S.; Pathak, T.; Zographos, S. E.; Oikonomakos, N. G. *Bioorg. Med. Chem.* **2006**, *14*, 6055.
- Samanta, A.; Leonidas, D. D.; Dasgupta, S.; Pathak, T.; Zographos, S. E.; Oikonomakos, N. G. *J. Med. Chem.* **2009**, *52*, 932.
- Thiyagarajan, N.; Smith, B. D.; Raines, R. T.; Acharya, K. R. *FEBS J.* **2011**, *278*, 541.
- Debnath, J.; Dasgupta, S.; Pathak, T. *Bioorg. Med. Chem.* **2009**, *17*, 6491.

20. Debnath, J.; Dasgupta, S.; Pathak, T. *Bioorg. Med. Chem.* **2009**, *17*, 4921.
21. Debnath, J.; Dasgupta, S.; Pathak, T. *Chemistry* **2012**, *18*, 1618.
22. Russo, A.; Acharya, K. R.; Shapiro, R. In *Methods of Enzymology*; Nicholson, A. W., Ed.; Academic Press: London, 2001; Vol. 341, pp 629–648.
23. Russo, N.; Shapiro, R. *J. Biol. Chem.* **1999**, *274*, 14902.
24. Stimac, A.; Kobe, J. *Carbohydr. Res.* **1992**, *232*, 359.
25. Lazrek, H. B.; Taourirte, M.; Oulih, T.; Barascut, J. L.; Imbach, J. L.; Pannecouque, C.; Witrouw, M.; De Clercq, E. *Nucleosides, Nucleotides Nucleic Acids* **1949**, *2001*, 20.
26. Vorbruggen, H.; Bennua, B. *Chem. Ber. Recl.* **1981**, *114*, 1279.
27. Hernandez, M. Z.; Cavalcanti, S. M.; Moreira, D. R.; de Azevedo, W. F., Jr.; Leite, A. C. *Curr. Drug Targets* **2010**, *11*, 303.
28. Russo, N.; Shapiro, R.; Vallee, B. L. *Biochem. Biophys. Res. Commun.* **1997**, *231*, 671.
29. Richards, F. M.; Wyckoff, H. W. *The Enzymes* **1971**, *4*, 647.
30. Iwahashi, K.; Nakamura, K.; Mitsui, Y.; Ohgi, K.; Irie, M. *J. Biochem. (Tokyo)* **1981**, *90*, 1685.
31. Beranek, J.; Hrebabecky, H. *Nucleic Acids Res.* **1976**, *3*, 1387.
32. Currid, P.; Wightman, R. H. *Nucleosides Nucleotides* **1997**, *16*, 115.
33. Bavaro, T.; Rocchietti, S.; Ubiali, D.; Filice, M.; Terreni, M.; Pregnotato, M. *Eur. J. Org. Chem.* **1967**, *2009*.
34. Kumar, V.; Malhotra, S. V. *Nucleosides, Nucleotides Nucleic Acids* **2009**, *28*, 821.
35. Yamamoto, Y.; Shimokawa, K.; Tanaka, K.; Hisanaga, Y. U.S. Patent 4847, **1989**, 366.
36. Sela, M.; Anfinsen, C. B. *Biochim. Biophys. Acta* **1957**, *24*, 229.
37. Anfinsen, C. B.; Redfield, R. R.; Choate, W. L.; Page, J.; Carroll, W. R. *J. Biol. Chem.* **1954**, *207*, 201.
38. Slifman, N. R.; Leogering, D. A.; McKean, D. J.; Gleich, G. J. *J. Immunol.* **1986**, *137*, 2913.
39. CrysAlisPro Software system, 2011. Agilent Technologies UK Ltd., Oxford, U.K.
40. CCP4. *Acta Crystallogr.* **1994**, *D 50*, 760.
41. Emsley, P.; Cowtan, K. *Acta Crystallogr., D: Biol. Crystallogr.* **2004**, *60*, 2126.
42. Adams, P. D.; Afonine, P. V.; Bunkoczi, G.; Chen, V. B.; Davis, I. W.; Echols, N.; Headd, J. J.; Hung, L. W.; Kapral, G. J.; Grosse-Kunstleve, R. W.; McCoy, A. J.; Moriarty, N. W.; Oeffner, R.; Read, R. J.; Richardson, D. C.; Richardson, J. S.; Terwilliger, T. C.; Zwart, P. H. *Acta Crystallogr., D: Biol. Crystallogr.* **2010**, *66*, 213.
43. Chen, V. B.; Arendall, W. B.; Headd, J. J.; Keedy, D. A.; Immormino, R. M.; Kapral, G. J.; Murray, L. W.; Richardson, J. S.; Richardson, D. C. *Acta Crystallogr., D: Biol. Crystallogr.* **2010**, *66*, 12.
44. Hubbard, S. J.; Thornton, J. M. Naccess V2.1.1 1993.
45. DeLano, W.L. *The PyMol Molecular Visualization System*, Sa Carlos, CA, USA, 2002.